ACS APPLIED MATERIALS & INTERFACES

Research Article

www.acsami.org

Liposomes Combined an Integrin $\alpha_v\beta_3$-Specific Vector with pH-Responsible Cell-Penetrating Property for Highly Effective Antiglioma Therapy through the Blood–Brain Barrier

Kairong Shi,[†] Yang Long,[†] Chaoqun Xu,[‡] Yang Wang,[†] Yue Qiu,[†] Qianwen Yu,[†] Yayuan Liu,[†] Qianyu Zhang,[†] Huile Gao,[†] Zhirong Zhang,[†] and Qin He*[,†]

[†]Key Laboratory of Drug Targeting and Drug Delivery Systems, West China School of Pharmacy, Sichuan University, No. 17, Block 3, Southern Renmin Road, Chengdu 610041, China

[‡]Sichuan Academy of Chinese Medicine Sciences, No. 51, Block 4, Southern Renmin Road, Chengdu 610041, China

Supporting Information

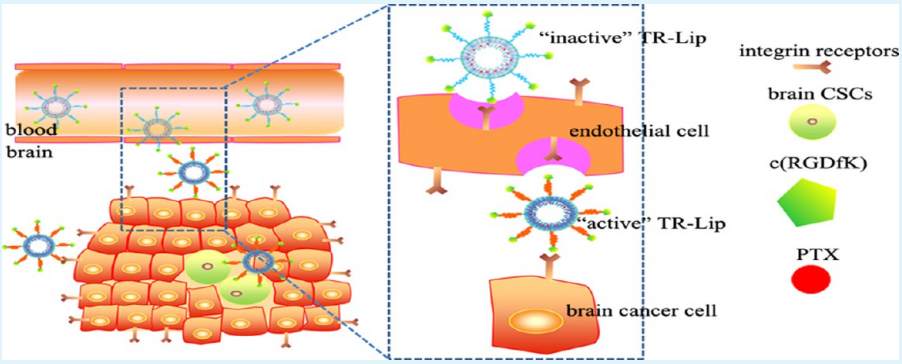

ABSTRACT: Glioma, one of the most common aggressive malignancies, has the highest mortality in the present world. Delivery of nanocarriers from the systemic circulation to the glioma sites would encounter multiple physiological and biological barriers, such as blood–brain barrier (BBB) and the poor penetration of nanocarriers into the tumor. To circumvent these hurdles, the paclitaxel-loaded liposomes were developed by conjugating with a TR peptide (PTX-TR-Lip), integrin $\alpha_v\beta_3$-specific vector with pH-responsible cell-penetrating property, for transporting drug across the BBB and then delivering into glioma. Surface plasmon resonance (SPR) studies confirmed the very high affinity of TR-Lip and integrin $\alpha_v\beta_3$. In vitro results showed that TR-Lip exhibited strong transport ability across BBB, killed glioma cells and brain cancer stem cells (CSCs), and destroyed the vasculogenic mimicry (VM) channels. In vivo results demonstrated that TR-Lip could better target glioma, and eliminated brain CSCs and the VM channels in tumor tissues. The median survival time of tumor-bearing mice after administering PTX-TR-Lip (45 days) was significantly longer than that after giving free PTX (25.5 days, $p < 0.001$) or other controls. In conclusion, PTX-TR-Lip would improve the therapeutic efficacy of brain glioma in vitro and in vivo.

KEYWORDS: *TR peptide, BBB penetrating, glioma targeting, cancer stem cells, VM channels*

1. INTRODUCTION

Glioma is one of the most aggressive and poorly treated intracranial tumors with high morbidity and mortality.[1−3] Because of the difficulty of completely removing glioma with surgical excision, irradiation and chemotherapy play vital roles in the treatment of glioma.[4−6] However, the treatment effect of chemotherapy still remains unsatisfied because of several limitations of chemotherapeutic agents, for example, systemic cytotoxic effects and limited drug penetration, which is attributed to the blood–brain barrier (BBB) and blood–brain tumor barrier (BTB).[2,4] Besides, heterogeneity of brain cancer such as cancer stem cells (CSCs) and vasculogenic mimicry (VM) may be another obstacle to cure tumor.[7] Brain CSCs, which have the capacity of self-renewal, proliferation, and high tumorigenicity, play a crucial role in tumor initiation, propagation, recurrence, and resistance to conventional chemotherapy.[8,9] VM, an alternative microvascular circulation independent of angiogenesis composed of endothelial cells, participates in many pathological processes including providing blood supply for the invasion and growth of brain cancer, demonstrating high resistance to drug, and rarely being removed by conventional chemotherapy.[10−12]

Considering the key role of BBB played in the physiological and pathological functions, a new brain drug delivery system with the long circulation lifetime, effective transport across intact BBB, and deep penetrating into tumor was necessarily

Received: July 16, 2015
Accepted: September 3, 2015
Published: September 15, 2015

DOI: 10.1021/acsami.5b06429
ACS Appl. Mater. Interfaces 2015, 7, 21442−21454

developed. In this regard, cyclic Arg-Gly-Asp (cRGD) was chosen as a candidate ligand because this peptide could selectively target integrin $\alpha_v\beta_3$-overexpressed on the endothelial cells[13,14] as well as glioma cells.[15,16] It was also reported that cRGD-modified nanocarriers had shown therapeutic efficacy on glioma-bearing mice,[6,13,17,18] whereas the penetration ability of cRGD-modified nanocarriers into the tumor parenchyma was poor.[19] To enhance the transport efficacy of cRGD-modified nanocarriers across BBB and simultaneously improve the penetration into the core of glioma, a "helper", who could help cRGD-modified nanocarriers escape efficiently from lysosomes in the endothelial cells and deep penetrate in the glioma, was needed. It was reported that histidine-rich TH peptide became protonated into positive charge under acid microenvironment around individual tumor cells from slightly negative at normal physiological condition because of the imidazole ring on histidine, which has a pK_a around 6.5.[20−23] Obviously, TH peptide would have the ability of proton sponge effect and pH-responsive cell penetrating property. TH-modified liposomes designed by our lab were also demonstrated to successfully escape from lysosomes in C26 cells and penetrate in the core of C26 tumor spheres at pH 6.3.[20,24] These suggested that TH peptide may satisfy the above-mentioned "helper". In view of this, a multifunctional peptide TR, a tandem peptide consisting of cRGD and TH peptide, was designed to not only have the ability of active targeting to integrin $\alpha_v\beta_3$, but also possess the capacity of cell penetrating peptide at tumor sites. It was hoped that TR peptide could not only guarantee efficient transcytosis after TR-conjugated cargo was internalized mediated by integrin $\alpha_v\beta_3$-overexpressed on the BBB, but also actively target and deep penetrate into the glioma.

On the basis of the above background, liposomes modified by TR (TR-Lip) were supposed to have the following characteristics (Figure 1): (1) TR-Lip could fast escape from lysosomes after

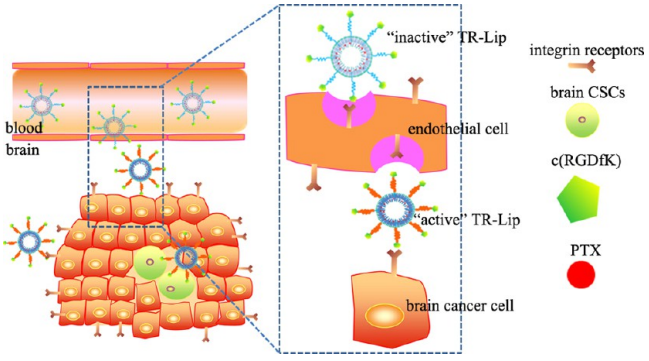

Figure 1. Schematic illustration of PTX-loaded TR-Lip across the BBB by receptor-mediated transcytosis and then directly delivering into glioma to kill brain cancer cells and CSCs. The "inactive" TR-Lip meant that TR-Lip with negative potential only had the ability of active targeting to integrin receptors during blood circulation. The "active" TR-Lip meant that TR-Lip with positive potential not only selectively targeted to glioma, but also could deep penetrate into glioma at tumor sites.

they were internalized by integrin $\alpha_v\beta_3$-overexpressing on BBB-mediated endocytosis due to proton sponge effect of TR-Lip in lysosomes; and (2) they then actively target and deep penetrate into glioma because the RGD fragment on the TR peptide enhanced the selective targeting of liposomes to integrin $\alpha_v\beta_3$-overexpressing cancer cells and simultaneously the TH fragment with the positive charge on the TR peptide improved cellular uptake of liposomes at tumor sites. In this study, transport efficacy and mechanism of TR-Lip across BBB were verified. The in vitro endocytosis, cytotoxicity of TR-Lip against C6 cells, CSCs, and VM channels under different pH conditions were investigated. Penetration in glioma spheroids in vitro also was studied. In vivo fate, and antitumor efficacy including eliminating brain cancer cells, brain CSCs, and VM channels, were also evaluated.

2. MATERIALS AND METHODS

2.1. Materials. SPC was purchased from Taiwei Chemical Co. (Shanghai, China). Cholesterol (Cho) was obtained from Chengdu Kelong Chemical Co. TR peptide with a terminal cysteine [c(RGDfK)-AGYLLGHINLHHLAHL(Aib)HHIL-Cys], TH peptide with a terminal cysteine (AGYLLGHINLHHLAHL(Aib)HHIL-Cys), and RGD with a terminal cysteine [c(RGDfK)-Cys] were synthesized by ZheJiang Ontores Biotechnologies Co. Ltd. (Hangzhou, China). 2-Dioleoyl-*sn*-glycero-3-phosp-hoethanolamine-*N*-(carboxyfluorescein) (CFPE), DSPE-PEG$_{2000}$-OMe, and DSPE-PEG$_{2000}$-Mal were obtained from Avanti Polar Lipids (Alabaster, AL). Coumarin-6, poly lysine, amiloride, chlorpromazine, filipin, sodium azide, and horseradish peroxidase (HRP) (RZ = 3.0−3.5, enzyme activity >265 U/mg, M_w = 44 kDa) were obtained from Sigma-Aldrich (St. Louis, MO). 3,3′,5,5′-Tetramethyl benzidine including H_2O_2 (TMB) was bought from Huzhou InnoReagents Co. Ltd. (Huzhou, China). 4′,6-Diamidino-2-pheylindole (DAPI), 1,1′-dioctadecyl-3,3,3′,3′-tetramethylindodicarbocyanine, and 4-chlorobenzenesulfonate salt (DiD) were purchased from Biotium (Hayward, CA). Transwells (6 wells, 1 μm pore size, polycarbonate membranes) were provided by Millipore (U.S.).

Male BALB/c mice were purchased from Sichuan University (Chengdu, China). All care and handling of animals was performed with the approval of the experiment animal administrative committee of Sichuan University.

2.2. Synthesis of DSPE-PEG$_{2000}$-Peptide. DSPE-PEG$_{2000}$-TR, DSPE-PEG$_{2000}$-TH were synthesized via conjugating DSPE-PEG$_{2000}$-Mal to the cysteine residue on TR and TH peptide, respectively. In brief, DSPE-PEG$_{2000}$-Mal and peptide were dissolved in mixed organic solvent chloroform/methanol (v/v = 2:1) at a 1.5:1 molar rate. The above mixed solution was stirred under nitrogen for 48 h at room temperature and traced by thin layer chromatography (TLC). The resulting reacting solution was dialyzed (MWCO = 3500, Biotopped, U.S.) against distilled H_2O for 48 h to remove excess peptide. The yielded product was lyophilized and stored at −20 °C until use. The products were confirmed by ^{1}H nuclear magnetic resonance (^{1}H NMR, 600 HMZ, Agilent Technologies 600/54 Premium Compact).

DSPE-PEG$_{2000}$-RGD was synthesized according to our previous publication.[5] In brief, DSPE-PEG$_{2000}$-Mal was dissolved into PBS (pH 8.0) to form micelle solution, and then c(RGDfK)-Cys was added to the above solution at a 2:1 molar rate. The reaction was maintained for 48 h at room temperature under moderate stirring and traced by TLC. The reaction mixture was then dialyzed (MWCO = 1000 Da) against distilled H_2O for 48 h to remove the unconjugated peptide. The final product was lyophilized and stored at −20 °C until use. The conjugation product DSPE-PEG$_{2000}$-RGD was confirmed by ^{1}H NMR.

2.3. Preparation and Characterization of Liposomes. Model probes (for example, CFPE, coumarin-6, and DiD) and PTX-loaded liposomes were prepared as in our previous report.[13] The constituents included SPC, Cho, DSPE-PEG$_{2000}$-OMe, DSPE-PEG$_{2000}$-peptide (59:33:2:6, molar ratio), and model probes or PTX. The final concentration of CFPE, coumarin-6, DiD, and PTX-loaded liposomes was 54, 10, 80, and 94 μM, respectively. The encapsulation efficiency (EE) of PTX-loaded liposomes was determined by high performance liquid chromatography (HPLC, Agilent 1200 series, Palo Alto, CA), and the drug-loading capacity (DL) was also calculated. The conventional liposomes were prepared by replacing DSPE-PEG$_{2000}$-peptide with DSPE-PEG$_{2000}$-OMe. The morphology of liposomes was observed by atomic force microscopy (AFM) (NSK Ltd., Tokyo, Japan). The particle sizes and zeta potential were measured via using the Malvern Zetasizer Nano ZS90 instrument (Malvern Instruments Ltd., UK).

DOI: 10.1021/acsami.5b06429
ACS Appl. Mater. Interfaces 2015, 7, 21442−21454

2.4. Surface Plasmon Resonance (SPR) Studies. TR-Lip binding affinities to integrin $\alpha_v\beta_3$ were evaluated by SPR using a Biacore T200 instrument at 25 °C (GE, U.S.) equipped with a CM5 chip under different acid conditions.[25,26] Integrin $\alpha_v\beta_3$ (R&D Systems, U.S.) was conjugated to a CM5 Biacore chip by amino coupling. The running buffers, 10 mM HEPES buffer (pH 7.4 or pH 6.5) containing 150 mM NaCl, 0.05% surfactant P-20 with 50 mM EDTA (HBS-Pp), were degassed prior to use. For SPR experiments, four kinds of liposomes were running at a flow rate of 10 μg/mL with an injection time of 30 s followed by a 3 min waiting time for dissociation. The running buffers (pH 7.4 or pH 6.5) were used as a negative control, respectively. All of the liposome concentrations diluted in running buffer were 30 nM. Data were analyzed using the Biacore T200 Control Software for binding affinity analysis of the liposomes and integrin $\alpha v\beta 3$.

2.5. Cell Culture. C6 cells (murine glioma cells), bEnd.3 cells (murine brain endothelial cells), and MCF-7 cells (human breast cancer cells) were cultured in Dulbecco's Modified Eagles Medium (DMEM) supplemented with 10% fetal bovine serum (FBS), 100 U/mL streptomycin, and 100 U/mL penicillin at 37 °C in a humidified 5% CO_2 atmosphere. For cells utilized for the assays at pH 6.5, the cells were preadapted to culture media of pH 6.5.

Glioma C6 cancer stem cells (CSCs) were grown in serum-free DMEM (Gbico, U.S.) supplemented with 2% B27 (Gibco), 20 ng/mL basic fibroblast growth factor, and 20 ng/mL epidermal growth factor (Macgene Biotech) as reported by Li et al.[7]

2.6. Blood−Brain Barrier (BBB) Model in Vitro. bEnd.3 cells were seeded on 6-well cell culture inserts at a density of 1×10^6 cells/insert, and cultured 7 days.[13] Before starting the experiment, the tight junctions of the monolayer were assessed by measuring the transendothelial electrical resistance (TEER) using a TEER instrument (Word Precision Instruments, Inc. Sarasota, FL) and viewed with a scanning electron microscope (SEM, JSM-5600 LV, JEOL, Japan). The permeability of the BBB model was evaluated by the amount of HRP across the BBB.[27]

2.6.1. Transport of Liposomes Across the BBB. To study the influence of different liposomes on the permeability on the BBB, several groups were set: CFPE-labeled PEG-modified liposomes (CFPE-PEG-Lip), CFPE-labeled RGD-modified liposomes (CFPE-RGD-Lip), CFPE-labeled TH-modified liposomes (CFPE-TH-Lip), and CFPE-labeled TR-modified liposomes (CFPE-TR-Lip). Permeability percent (P%) was calculated to evaluate the effect of peptide-modified liposome on transporting model probe (CFPE) across the BBB.[28]

2.6.2. Immunohistochemistry Staining. To investigate the effect of various PTX formulations on the BBB, tight junctions presented among bEnd.3 cells were visualized through immunostaining of ZO-1 expression.[29,30] Briefly, bEnd.3 cells were incubated to allow the confluence to reach greater than 100%. After the treatment with PTX formulations (10 μM) for 60 min, the cells were rinsed, fixed, blocked, and incubated with rabbit antimouse ZO-1 primary antibody (Capital-Bio Corp., China), then incubated with Alexa-Fluoro 594-conjugated donkey antirabbit secondary antibody (Jackson ImmunoResearch, West Grove, PA). The nuclei were stained with DAPI and were imaged with a laser scanning confocal microscope (CLSM) (TCS SP5 AOBS confocal microscopy system, Leica, Germany).

2.6.3. Intracellular Trafficking of Liposomes. For evaluating lysosomal escape ability of liposomes, lysosomes were staining to colocalize liposomes. Briefly, bEnd.3 cells were incubated with CFPE-labeled liposomes for 1.5 h, then treated with Lyso-Tracker (Invitrogen, Carlsbad, CA) for 0.5 h. After that, the nuclei were stained with DAPI, and the cells were imaged with CLSM.

2.7. Western Blot Analysis. For obtaining the purified braining CSCs, a magnetic-associated cell sorting (MACS) was used. Briefly, $CD44^+$ CSCs were isolated from C6 CSCs by MACS, which was that C6 mammospheres were collected, washed in PBS, dissociated with trypsin, and washed. $CD44^+$ subsets were isolated by using microbeads conjugated to monoclonal antimouse CD44 antibodies (Miltenyi Biotec., Germany). To increase the purity of $CD44^+$ cells, the eluted fraction from the column should be directly enriched over a second column for repeating the magnetic separation again. The resulting $CD44^+$ cells were labeled "C6 CSCs". C6 CSCs were identified using another specific procedure. In brief, for Western blot analysis of $CD133^+$ protein expression, which was overexpressed on the C6 CSCs as compared to glioma C6 cells, 40 μg of total cell lysate was separated by 10% SDS-PAGE and transferred onto nitrocellulose membranes by electroblotting. The membranes were blocked in 5% milk powder in 0.05% Tween-20 TBST for 2 h and probed with antibodies against CD 133 (1:500) overnight at 4 °C or GAPOH (1:2500) for 1 h at room temperature. After 2 h of incubation with horseradish peroxidase-coupled secondary goat antirabbit (1:1000), specific antibody binding was detected by using the enhanced chemiluminescence technique on a Bio-Rad ChemiDoc MP System (Bio-Rad Laboratories, U.S.). Glioma C6 cells were used as negative controls for the Western blot experiments.

2.8. Cellular Uptake of Liposomes. For flow cytometry studies, C6 cells, MCF-7 cells, and C6 CSCs were seeded onto a six-well plate at a density of 1×10^6 cells/well and incubated under 37 °C for 24 h. Cells were incubated with CFPE-labeled liposomes for 2 h under different acid conditions (pH 7.4 and pH 6.5), the cells were washed with cold PBS three times, then trypsinized, centrifugated, and resuspended. The fluorescent intensity of cells was analyzed by a flow cytometer (Cytomics FC 500, Beckman Coulter, Miami, FL). Ten thousand cells were recorded for each sample.

For confocal microscope studies, C6 cells and MCF-7 cells were plated onto a six-well plate containing cover glass at a density of 1×10^5 cells/well. After 24 h incubation, CFPE-labeled liposomes were employed to each well and allowed for further coincubation for 2 h under different pH conditions (pH 7.4 or pH 6.5). Following that, the cells were rinsed with cold PBS three times and fixed with 4% paraformaldehyde for 30 min at room temperature, and then cell nuclei were stained with DAPI for 15 min. Finally, the samples were imaged using CLSM.

2.9. Endocytosis Pathways. To explore the endocytosis pathway of TR-Lip on C6 cells at pH 6.5, endocytosis inhibition assay was employed. Briefly, the cells were preincubated with amiloride, chlorpromazine, filipin, polylysine (PLL), free RGD peptide, and free RGD + PLL for 0.5 h at 37 °C, respectively. The culture medium containing the inhibitors then was discarded, and fresh culture media containing CFPE-labeled liposomes were used for another 1.5 h incubation at pH 6.5. The cells were determined quantitatively by flow cytometer and were imaged qualitatively by CLSM.

2.10. Antiproliferative Activity against C6 Glioma Cells and C6 CSCs. Glioma C6 cells were seeded at 5000 cells/well and grown in serum-containing culture medium at 37 °C for 24 h in a humidified 5% CO_2 atmosphere. The medium was replaced with serum-free culture media (pH 7.4 and pH 6.5) containing varying concentrations of PTX-loaded PEG-, RGD-, TH-, TR-modified liposomes, and free PTX. The final concentration of PTX was 0−20 μg/mL. After 2 h, the above drug-containing culture medium was then replaced with serum-containing culture medium and continually cultured for 22 h. At 24 h, cell viability was determined by 3-(4,5-dimethyl-2-thiazolyl)-2,5-diphenyl-2-*H*-tetrazolium bromide (MTT) at 570 nm using a microplate reader (Thermo Scientific Varioskan Flash, U.S.). Survival (%) was calculated using the following formula: cell viability (%) = $A_{test}/A_{control} \times 100\%$, where A_{test} and $A_{control}$ represented the absorbance of cells treated with different test solutions and blank culture media, respectively. The viability of C6 cells treated with various blank liposomes was determined as that described above as well.

The cytotoxicity of C6 CSCs was also evaluated, where the operating procedure was identical to that employed for glioma cells.

2.11. Destruction of C6 Vasculogenic Mimicry (VM). The destroying effect on the VM channels of glioma C6 cells was employed to assess the activity of PTX-loaded liposomes or free PTX under acid conditions. Briefly, 150 μL of Matrigel was plated onto 24-well plates, and incubated for 1 h at 37 °C until Matrigel solidification. Glioma C6 cells (1×10^4) were resuspended with serum-free DMEM and then loaded on the top of the Matrigel. After incubation at 37 °C for 8 h, the above culture medium was replaced with serum-free DMEM with different acid medium containing free PTX, PTX-PEG-Lip, PTX-RGD-Lip, PTX-TH-Lip, and PTX-TR-Lip, respectively. The final concentration of PTX was 1 μM. After incubation at 37 °C for 2 h, each well was analyzed directly under Carl Zeiss 40CFL Axiovert 40 inverted microscopy (Germany).

DOI: 10.1021/acsami.5b06429
ACS Appl. Mater. Interfaces 2015, 7, 21442−21454

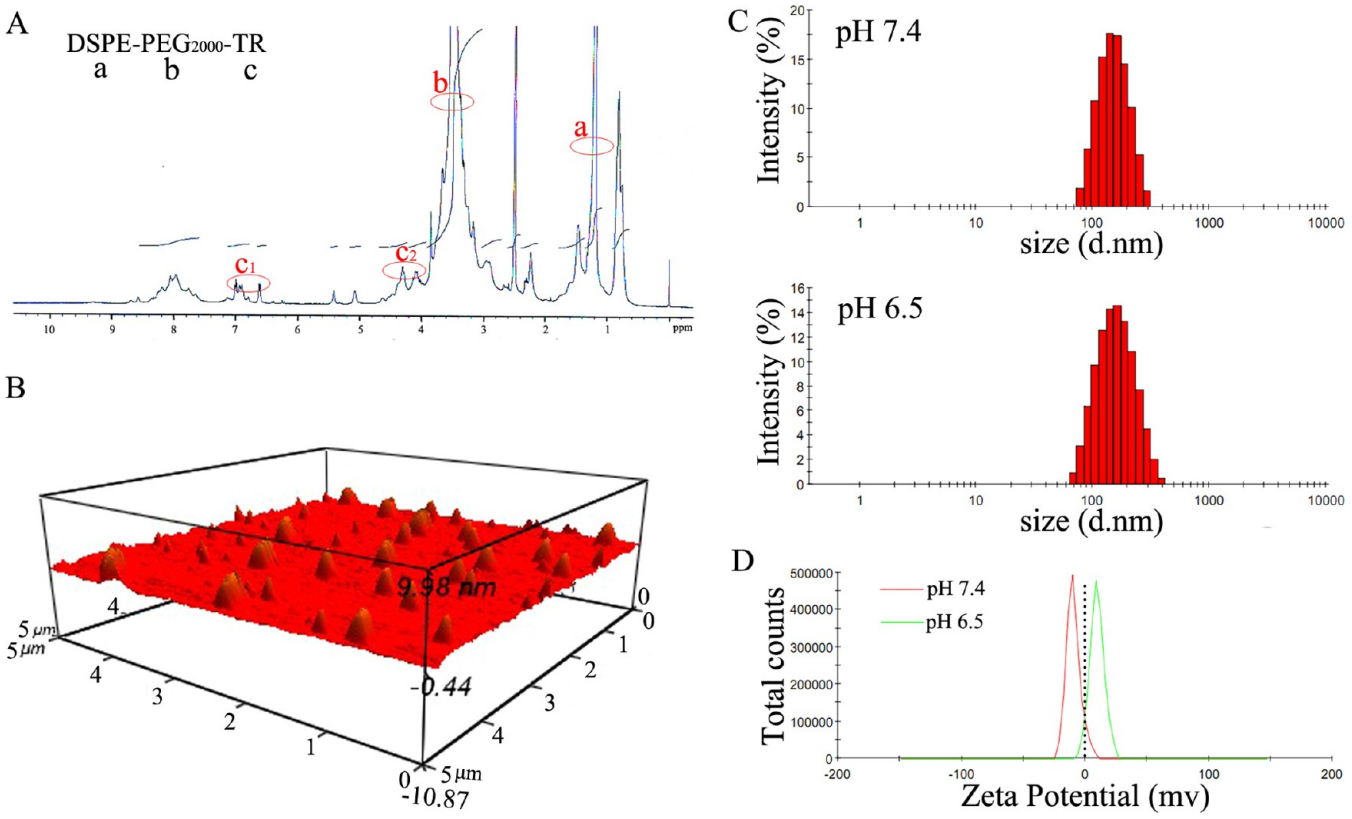

Figure 2. (A) ^{1}H NMR spectrum of DSPE-PEG$_{2000}$-TR in DMSO. (B) AFM image of TR-Lip. (C) Size of TR-Lip by DLS under different pH conditions. (D) Charge reverse of TR-Lip from negative potential at pH 7.4 to positive at pH 6.5.

Table 1. EE, Particle Sizes, Zeta Potentials, PDI, and DL of PTX-Loaded Liposomes under Different pH Conditions[a]

		EE (%)	zeta potential (mV)	size (nm)	PDI	DL (%)
PTX-PEG-Lip	pH 7.4	93.02 ± 0.515	−18.4 ± 1.37	102.7 ± 2.530	0.214 ± 0.012	3.35 ± 0.54
	pH 6.5		−17.7 ± 0.628	105.1 ± 2.302	0.215 ± 0.024	
PTX-RGD-Lip	pH 7.4	93.27 ± 0.481	−14.2 ± 1.02	110.2 ± 0.571	0.185 ± 0.033	3.21 ± 0.41
	pH 6.5		−13.2 ± 1.20	109.8 ± 1.54	0.206 ± 0.021	
PTX-TH-Lip	pH 7.4	94.30 ± 0.580	−5.06 ± 1.01	127.4 ± 0.545	0.231 ± 0.013	3.24 ± 0.52
	pH 6.5		3.20 ± 1.24	128.0 ± 0.243	0.244 ± 0.018	
PTX-TR-Lip	pH 7.4	93.28 ± 0.325	−3.71 ± 0.86	131.8 ± 0.729	0.239 ± 0.011	3.29 ± 0.50
	pH 6.5		9.50 ± 1.32	130.3 ± 1.425	0.254 ± 0.025	

[a] n = 3, mean ± SD.

2.12. Penetrating Ability to Brain Tumor Spheroids. Avascular spheroids of C6 glioma cells were grown to in vitro evaluate the tumor penetrating ability of liposomes.[31,32] Briefly, 50 μL of 2% agarose solution (w/v) was placed onto each well of a 96-well culture plate and solidified. Glioma C6 cells (5×10^3) were resuspended with DMEM and then seeded on the top of the agarose. The cells were cultured at 37 °C in a humidified atmosphere containing 5% CO_2. After 5 days, the formed tumor spheroids were incubated with coumarin-6-labeled PEG-Lip, RGD-Lip, TH-Lip, and TR-Lip under different pH conditions, respectively. The final concentration of coumarin-6 was 10 μM. After 2 h, the spheroids were rinsed with PBS and fixed with 4% paraformaldehyde for 30 min before subjection to CLSM. The penetrative depth between the different layers from the top of the spheroid to the middle was 20 μm.

2.13. In Vivo Image. The C6 cells (1×10^6 cells/5 μL) were injected into corpus striatum of female BALB/c mice (18−20 g) as previously described.[33] After 14 days, the mice were randomly divided into five groups (3 each group) and were intravenously injected via the tail of the tumor-bearing mice with PBS, DiD-PEG-Lip, DiD-RGD-Lip, DiD-TH-Lip, and DiD-TR-Lip. The mice then were scanned at 1, 8, and 24 h using IVI Spectrum system (Caliper, Hopkington, MA).

For further observing the distribution of different liposomes in tumor masses and the major organs, the tumor-bearing mice were sacrificed after heart perfusion with PBS and 4% paraformaldehyde at the end of the in vivo imaging. Following that, the brain, heart, liver, spleen, lung, and kidney were immediately collected and photographed.

2.14. Anticancer Efficacy. *2.14.1. Survival of Gloma-Bearing Mice.* At the eighth day after tumor inoculation, the mice were randomly divided into 6 groups (10 per group). The mice in the blank control group were administered with PBS. The mice in the other 5 groups were treated with free PTX, PTX-PEG-Lip, PTX-RGD-Lip, PTX-TH-Lip, and PTX-TR-Lip via tail vein at a dose of 3 mg/kg PTX, respectively. Administration was made every 2 days with a total of 5 doses per mice. At day 18, 2 mice from each group were killed for immunohistochemical observation (for example, hematoxylin and eosin (H&E) staining, brain CSCs, brain cancer VM channels), and the other eight mice were used for monitoring the survival curves. The survival time was calculated from the day of tumor inoculation to the day of death. Kaplan−Meier survival curves were plotted for each group.

2.14.2. Brain CSCs. CD133 is a CSC marker in malignant brain tumors.[34] To evaluate the efficacy of different PTX formulations against brain CSCs in vivo, the immunoperoxidase method was used to carry

DOI: 10.1021/acsami.5b06429
ACS Appl. Mater. Interfaces 2015, 7, 21442−21454

out immunohistochemical staining using anti-CD133 antibody. Immunohistochemical reactions were visualized with horseradish peroxidase. Nuclei were counterstained with hematoxylin, then dehydrated and sealed with a coverslip.

2.14.3. Brain Cancer VM Channels. To access the destruction of different PTX formulations against brain VM channels in vivo, mouse monoclonal anti-CD34 and periodic acid-schiff (PAS) were used to visualize the formed VM channels. Positive and negative controls without primary antibody were included.

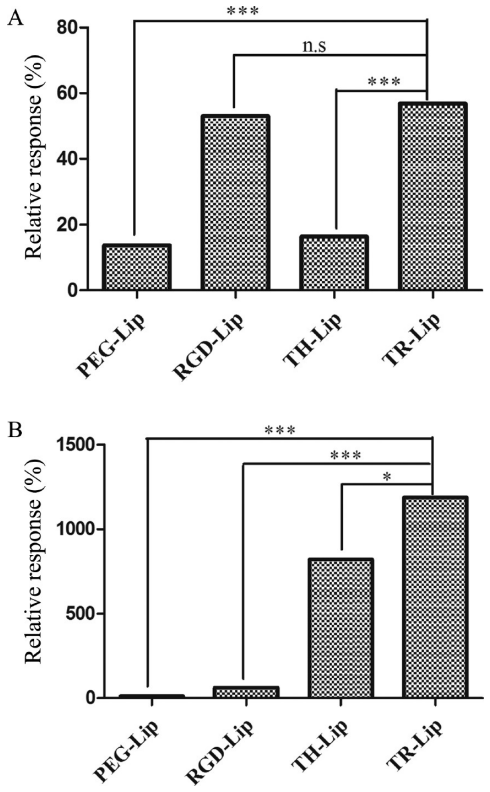

Figure 3. SPR analysis measuring liposomes binding to integrin $\alpha_v\beta_3$ at pH 7.4 (A) and pH 6.5 (B), respectively.

2.15. Statistical Analysis. The results were reported as means ± SD. The Student's *t* test or one-way ANOVA was used to determine statistical significance. Statistical significance was set at $^*p < 0.05$, and extreme significance was set at $^{**}p < 0.01$

3. RESULTS AND DISCUSSION

3.1. Characterization of Liposomes. To prepare peptide-modified liposomes, RGD-PEG$_{2000}$-DSPE, TH-PEG$_{2000}$-DSPE, and TR-PEG$_{2000}$-DSPE were first synthesized and characterized by ^{1}H NMR spectrum as shown (Figure 2A and Figure S1). The appearance of characteristic peaks at 1.2−1.4 ppm (peak a) and 3.4−3.8 ppm (peak b) indicated the existence of DSPE and PEG$_{2000}$ in the conjunct of DSPE-PEG$_{2000}$-TR, respectively. The multiplets at 4.0−4.4 ppm (peak c_2) and 6.8−7.0 ppm (peak c_1) were attributed to the c(RGDfK) and TH fragment of TR block in the above conjunct, respectively. These data indicated that TR peptide was successfully conjugated to the end of the distal end of Mal-PEG$_{2000}$-DSPE by a nucleophilic substitution reaction. A schematic drawing of TR-Lip was shown in Figure 1. The AFM of TR-Lip showed a smooth surface of approximately 130 nm in diameter (Figure 2B). The size and zeta potential distribution graphs of PTX-TR-Lip were shown in Figure 2C and D under different acid conditions, respectively.

Table 1 displayed EE, zeta potential, particle size, polydispersity index (PDI), and DL of PTX-loaded liposomes under different pH conditions. As compared to PEG-Lip, TR-Lip showed a slightly larger size due to the modification of DSPE-PEG$_{2000}$-TR. TH-Lip and TR-Lip turned positive potential at pH 6.5 from negative at pH 7.4, due to the protonation ability of the imidazole ring on the TH and TR peptide at pH 6.5.[35] The in vitro release percentages at 6.5 and 7.4 at 24 h were (32.26 ± 2.91)% and (30.43 ± 2.16)%, respectively. The release profile of TR-Lip displayed similar features with our previous report of PEG-Lip, RGD-Lip, and TH-Lip, indicating that the release profile of TR-Lip was not affected by pH-responsive TR modification.

3.2. SPR Analysis. To evaluate TR-Lip for binding affinities to integrin $\alpha_v\beta_3$, we functionalized integrin $\alpha_v\beta_3$ to the surface of

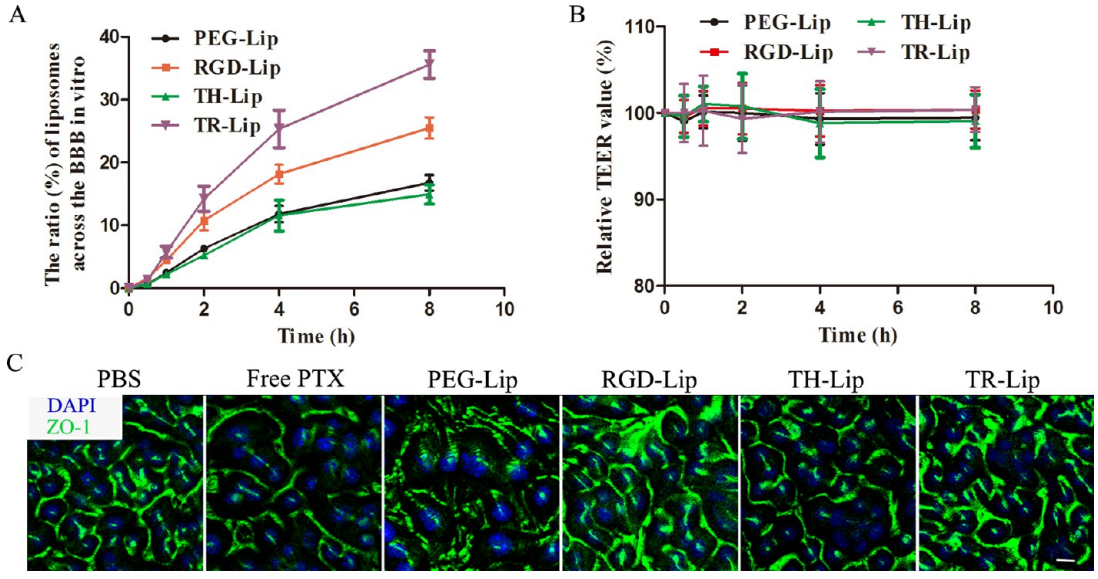

Figure 4. Transport ratios (%) (A) and the change of TEER values (B) of FITC-labeled liposomes across the BBB in vitro during 8 h. (C) Immunofluorescence microscopic images of tight junction-associated protein ZO-1 after 60 min treatment with PBS, free PTX, PTX-PEG-Lip, PTX-RGD-Lip, PTX-TH-Lip, and PTX-TH-Lip. Nuclei and ZO-1 are displayed in blue and green, respectively. Data are means ± SD (n = 3). Scale bar, 10 μm.

DOI: 10.1021/acsami.5b06429
ACS Appl. Mater. Interfaces 2015, 7, 21442−21454

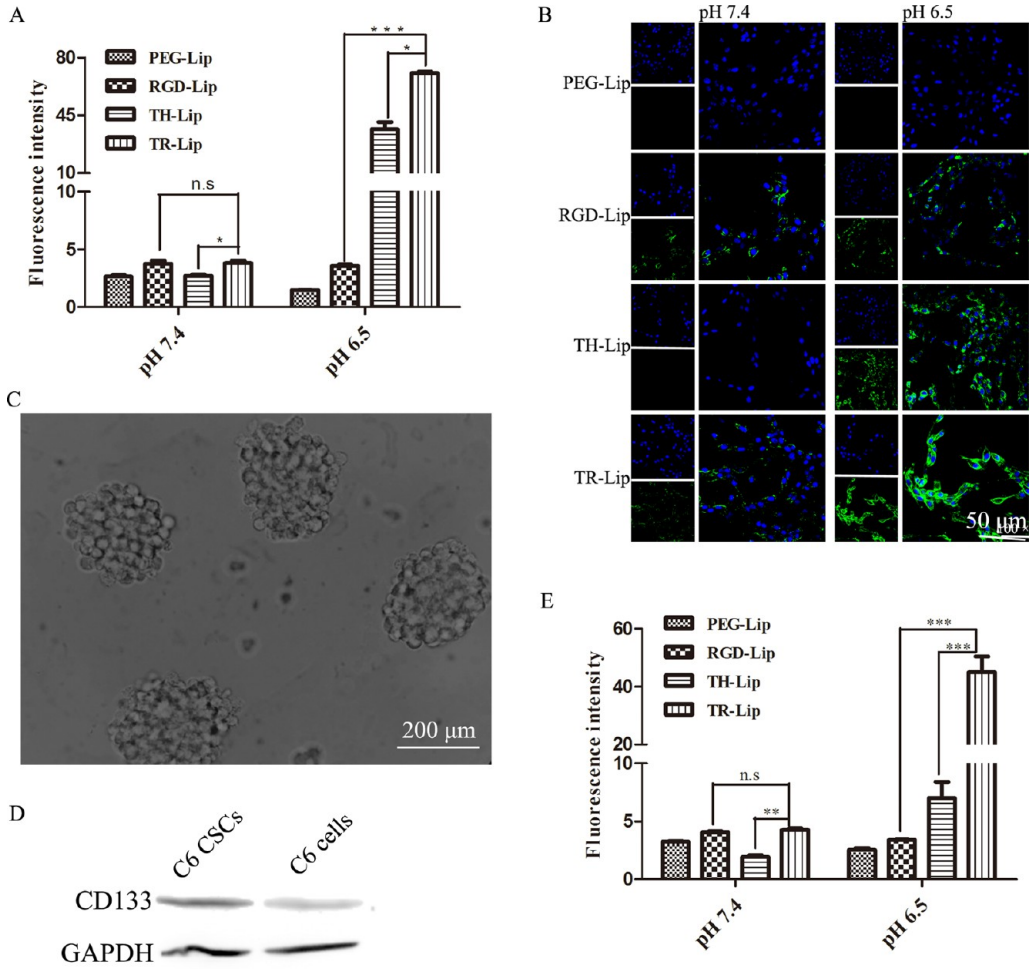

Figure 5. Quantitative (A) and qualitative (B) cellular uptake of CFPE-labeled liposomes on C6 cells. Scale bar, 50 μm. Phenotypic and morphological identification of C6 CSCs: microscopic image of C6 CSCs spheres (C), phenotypic identification of C6 CSCs by Western blot (D). (E) The cellular uptake of C6 CSCs after treatment with CFPE-labeled liposomes at 2 h under different pH conditions. Data were the mean ± SD (n = 3). *p < 0.05, **p < 0.01, ***p < 0.001.

a CM5 chip and evaluated the binding of various liposomes under different pH conditions. As compared to the nonspecific binding of PEG-Lip, both TR-Lip and RGD-Lip showed similar specific binding to integrin $\alpha_v\beta_3$ at pH 7.4 (Figure 3A). Interestingly, as compared to RGD-Lip and TH-Lip, TR-Lip bound strongly to integrin $\alpha_v\beta_3$ at pH 6.5 (Figure 3B), and the absorbed TR-Lip did not significantly desorb from the integrin $\alpha_v\beta_3$ with standard Biacore regeneration procedures (data not shown). All of these data suggested strong specific interactions between TR-Lip and integrin $\alpha_v\beta_3$, and the highly specific binding of TR-Lip made an important proof-of-concept determination in this study.

3.3. Transport of Liposomes Across the BBB. To evaluate the establishment of the BBB model in vitro, the morphology and permeability of the BBB model in vitro were measured (Figure S2A and B).[27,36] SEM showed the tight junctions among cells. TEER value of bEnd.3 monolayer was higher than 250 Ω cm^2, and the permeability of HRP on the BBB model in vitro was less than 3% during 8 h.

Figure 4A showed the transport ratios of the liposomes across the BBB model in vitro within 8 h. The transport ratios of TR-Lip (35.59 ± 2.18%) were higher than those of PEG-Lip (16.78 ± 1.24%), RGD-Lip (25.48 ± 1.70%), and TH-Lip (14.96 ± 1.54%). Additionally, it was also observed that the TEER values

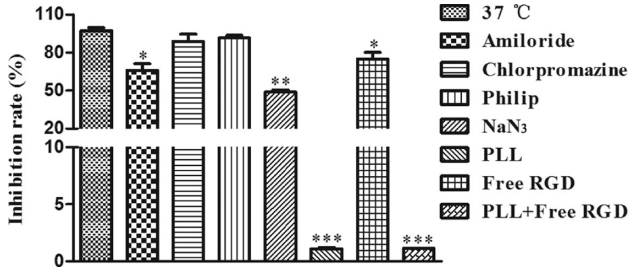

Figure 6. Endocytosis inhibition assay on C6 cells at pH 6.5. These histograms showed the inhibition rates of different inhibitors on C6 cells (n = 3, mean ± SD). *p, **p, and ***p indicated p < 0.05, p < 0.01, and p < 0.001 versus control group (37 °C), respectively.

of the above bEnd.3 monolayers did not change obviously over time with the incubation of liposomes, indicating that the integrity of cell monolayer was not disrupted and the translocation was only through a transcellular pathway (Figure 4B). Figure S2C also verified our hypothesis that TH fragment on TR peptide could help TR-Lip escape from lysosomes in bEnd.3 cells, suggesting that TR-Lip would have higher transport efficacy than RGD-Lip, which might be trapped in lysosomes, making endosome escape a key limitation. The results indicated that the

DOI: 10.1021/acsami.5b06429
ACS Appl. Mater. Interfaces 2015, 7, 21442−21454

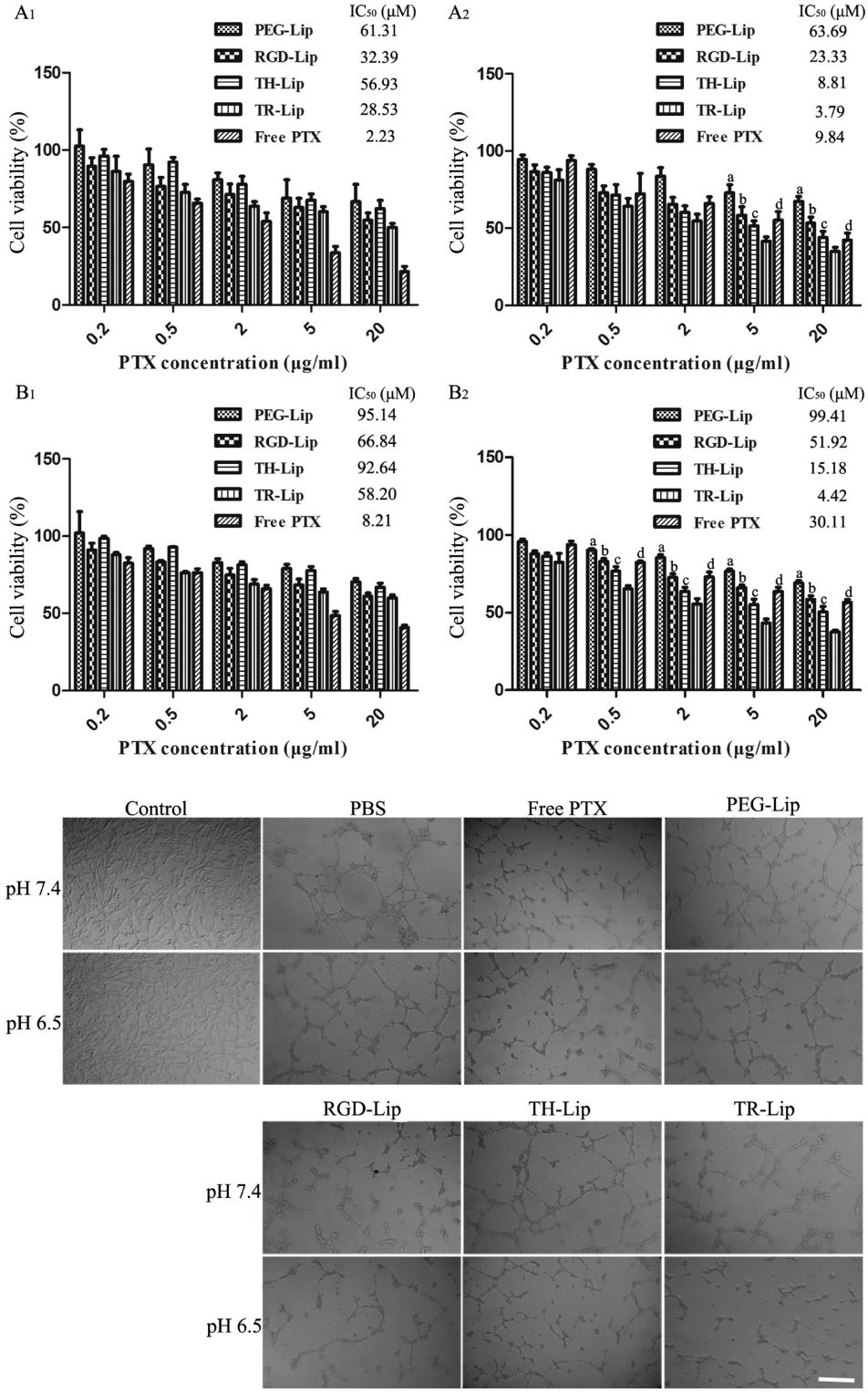

Figure 7. Cell viability (%) of C6 cells (A1, A2) as well as C6 CSCs (B1, B2) after treatment with various formulations at pH 7.4 and at pH 6.5, respectively. Data were the mean ± SD (n = 3). a, $p < 0.001$, versus PTX-PEG-Lip; b, $p < 0.001$, versus PTX-RGD-Lip; c, $p < 0.001$, versus PTX-TH-Lip; d, $p < 0.001$, versus free PTX. (C) Destruction of brain cancer VM channels after treatment with various formulations. Scale bar, 500 μm.

transport of TR-Lip across the BBB was significantly increased when liposomes were coupled with TR peptide.

Figure 4C did not show significantly discontinued intervals and even the obvious absence of protein ZO-1 after treatment of PTX-loaded formulations except free PTX. The above data indicated that PTX-TR-Lip would not disrupt tight junctions among adjacent cells. BBB is the most important barrier in preventing invading organisms and unwanted substances from reaching the brain parenchyma and providing a sanctuary for the central nervous system.[37] It is reported that more than 98% of small molecules including therapeutics do not cross the BBB, and disrupting the BBB carries the risk of epileptic seizures and

DOI: 10.1021/acsami.5b06429
ACS Appl. Mater. Interfaces 2015, 7, 21442−21454

neurotoxicity.[30,38] Therefore, TR-Lip may be a safe and effective delivery system of drugs for the treatment of glioma.

3.4. Cellular Uptake. C6 cells (positive-expressed integrin $\alpha_v\beta_3$) and MCF-7 (negative-expressed integrin $\alpha_v\beta_3$) were chosen to evaluate the targeting efficiency of TR-Lip under different acid conditions.[39,40] Figure 5A depicted that the uptake of TR-Lip was 48.06-, 19.76-, and 1.93-fold higher than that of PEG-Lip, RGD-Lip, and TH-Lip at pH 6.5, respectively; it was also seen that there was no significant difference in uptake between TR-Lip and RGD-Lip at pH 7.4 on C6 cells. Figure S4 displayed that the uptake of TR-Lip on MCF-7 cells was 18.78-, 15.55-, and 1.03-times higher than that of PEG-Lip, RGD-Lip, and TH-Lip at pH 6.5, respectively, whereas all liposomes showed similar uptake on MCF-7 at pH 7.4. The images by CLSM (Figure 5B and Figure S4B) were well consistent with the above results by a flow cytometer. All data showed that TR-Lip had better targeting property to integrin $\alpha_v\beta_3$-expressed C6 at pH 6.5 due to the synergistic effect of the receptor- and electrostatic-mediated endocytosis.

Figure 5C and D showed the morphological identification of brain glioma stem cells and the phenotype (marked CD 133$^+$).[7] The uptake of TR-Lip on C6 CSCs was 17.84-, 13.11-, and 6.43-times higher than that of PEG-Lip, RGD-Lip, and TH-Lip at pH 6.5, respectively (Figure 5E). Obviously, TR-Lip could be more easily internalized into C6 CSCs, which could be explained as follows: C6 CSCs were more sensitive to liposomes modified by TR peptide at pH 6.5.

3.5. Endocytosis Pathways. The endocytosis pathway of TR-Lip on C6 cells at pH 6.5 after treatment with different inhibitors was evaluated by quantitative and qualitative research (Figure 6 and Figure S3). Both the presence of chlorpromazine, an inhibitor of clathrin vesicles, and philip as the inhibitor of caveolae did not significantly prevent the cellular uptake of TR-Lip.[41] The cellular uptake after treatment with amiloride (an inhibitor of macropinocytosis) and NaN_3 (energy inhibitor) decreased by 32.08% ($p < 0.05$) and 49.92% ($p < 0.01$), respectively, suggesting that macropinocytosis-mediated and energy-dependent endocytosis played an important role in the cellular uptake of TR-Lip.[42,43] The preadded free RGD peptide also competitively inhibited the cellular association of TR-Lip ($p < 0.05$), confirming the contribution of RGD fragment on the TR modification to the enhanced cellular uptake.[44] Furthermore, the cellular uptake of groups treatment with PLL and PLL + free RGD significantly decreased by 98.83% and 98.81%, respectively, suggesting TH fragment on TR peptide played a vital role in cellular uptake as compared to RGD fragment on TR peptide.

3.6. In Vitro Cytotoxicity Study on C6 Cells and C6 CSCs. It was shown that all of the blank liposomes under different acid conditions exhibited little toxicity (Figure S5). Figure 7A and B displayed the antiproliferative effect of PTX-TR-Lip on C6 cells and C6 CSCs under different acid conditions, respectively. The results from MTT assays showed that PTX-TR-Lip exhibited the strongest inhibitory effect on the proliferation of C6 cells and C6 CSCs among various formulations at pH 6.5.

The IC_{50} values of PTX-TR-Lip against C6 cells and C6 CSCs were 3.79 ± 0.19 and 4.42 ± 0.23 μM at pH 6.5, respectively. The IC_{50} value of PTX-TR-Lip against C6 cells was 16.80-, 6.15-, 2.32-, and 2.60-fold lower than that of PTX-loaded PEG-Lip, RGD-Lip, TH-Lip, and free PTX at pH 6.5, respectively. However, the IC_{50} value of PTX-TR-Lip against C6 CSCs was 22.49-, 11.74-, 3.43-, and 6.78-fold lower than that of

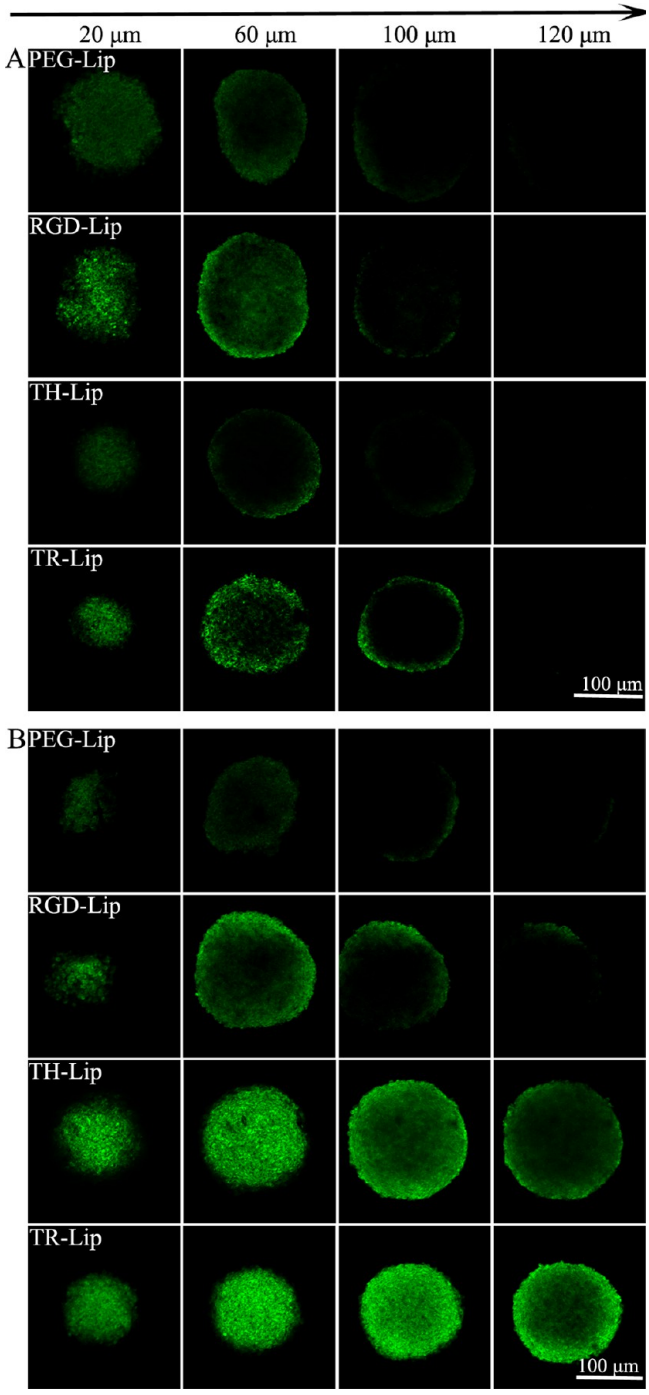

Figure 8. Penetrating ability of various formulations into C6 tumor spheres at (A) pH 7.4 and (B) pH 6.5. Scale bar, 100 μm.

PTX-loaded PEG-Lip, RGD-Lip, TH-Lip, and free PTX at pH 6.5, respectively. One key impact of the elevated IC_{50} values of other formulations against CSCs except PTX-TR-Lip could be relevant with the roles of CSCs in resistance to therapy.[45] Thus, PTX-TR-Lip had the greatest antiproliferative effects against C6 cells and C6 CSCs growth as compared to free PTX and other formulations at pH 6.5. The enhanced inhibitory effect could be attributed to the higher intracellular uptake (Figure 5A and E) as well as overcoming multidrug resistant (MDR) via changing endocytosis pathways of PTX-loaded liposomes by modifying with TR peptide.

DOI: 10.1021/acsami.5b06429
ACS Appl. Mater. Interfaces 2015, 7, 21442−21454

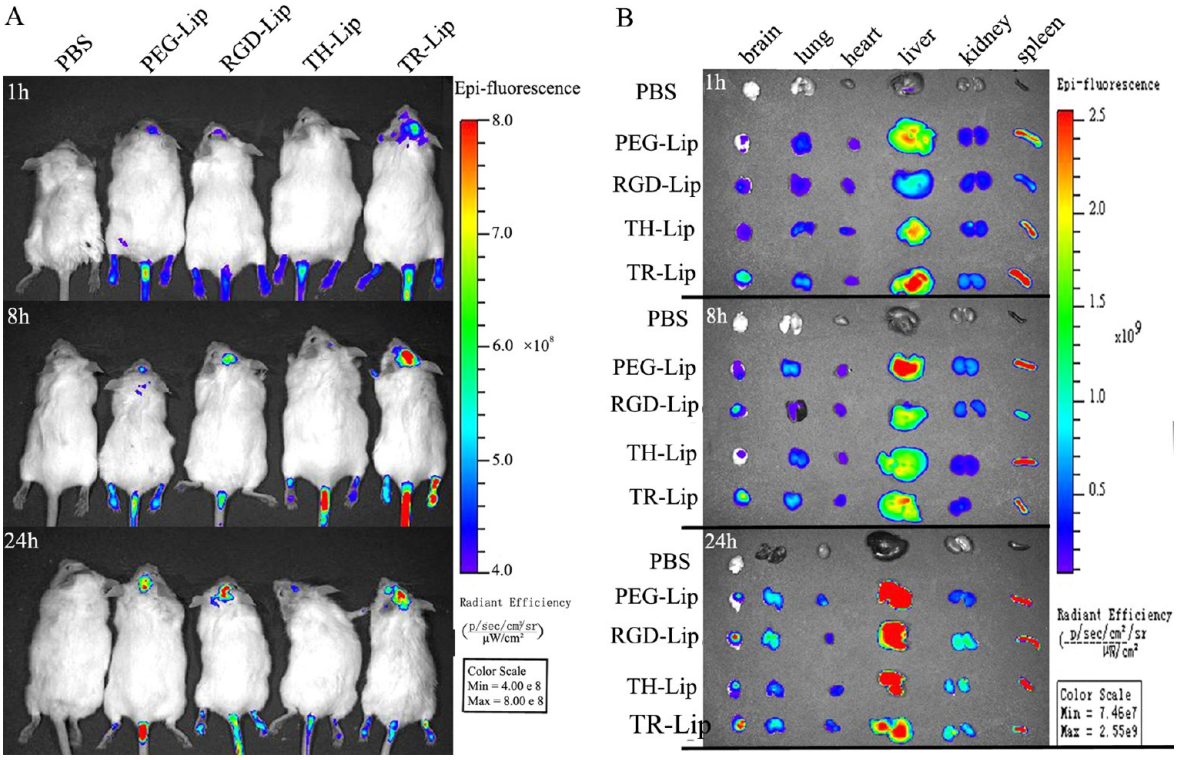

Figure 9. (A) In vivo near-infrared imaging of mice treated with DiD-labeled liposomes. In vivo images were taken at 1, 8, and 24 h after iv injection. (B) Ex vivo images showed the corresponding exposed main organs (glioma-bearing brain, lung, heart, liver, kidney, spleen) that were excised after imaging in vivo.

3.7. Destruction of Brain Cancer VM Channels. VM channels composed of tumor cells might help tumor cells obtain sufficient oxygen and enough nutrients supply.[7,10] It was therefore necessary to evaluate the activity of PTX-TR-Lip against the VM channels composed of glioma C6 cells. The C6 cells formed vessel-like loops, channels, and networks in three-dimensional Matrigel under different pH conditions (Figure 7C (PBS) versus (control) without three-dimensional Matrigel). After treatment with different formulations, the destruction of VM channels formed in three-dimensional Matrigel was displayed (Figure 7C). PTX-TR-Lip showed the strongest destroying effect at pH 6.5 as compared to other formulations, suggesting that TR-Lip would be a potential platform for targeting to the VM channels of brain glioma C6 cells. Little is known about the molecular mechanisms of VM involving dysregulation of the tumor-specific phenotype and the concomitant transdifferentiation of aggressive tumor cells into other cell types. FAK, EPHA2, VE-cadherin, MMPs, laminin 5 γ2-chain, and NOTCH proteins as components of the vasculogenic switch are targets to inhibit the formation of VM channels.[10,11,46]

3.8. Penetration in Avascular C6 Glioma Spheroids. Avascular spheroids, 3D in vitro microscale tissue analogues, have sizable cell−cell interactions, increased interstitial pressure, and diffusional limitations of drugs. Spheroids serve as an ideal format in vitro for studies of drug penetration because of their mimicry of the physiological barriers to drug delivery in vivo.[47] Penetrating efficacy of TR-Lip was evaluated in avascular C6 glioma spheroids under different pH conditions. Figure 8 depicted that TR-Lip penetrated deepest and distributed most extensive in the C6 glioma spheroids at pH 6.5, suggesting that TR-Lip could be faster internalized into C6 cells than other controls and might penetrate through cell by cell into the deep tumor spheroids. To prevent the recurrence of cancer due to rare cells (e.g., cancer stem cells or primary stem cells) incorporated and maintained in tumor in vivo, the penetrating ability of TR-Lip would be an excellent drug delivery system for enhancing the amount of drug accessing the inside of the solid tumors.[32,47]

3.9. Imaging in Vivo. To evaluate the glioma-targeting effect of TR-Lip, glioma-bearing mice were employed. TR-Lip showed the strongest accumulation in glioma from 1 to 24 h after administration (Figure 9A), suggesting that TR was a key to deliver liposomes into orthotopic brain tumor models across BBB. Images of the isolated organs showed much stronger fluorescent intensity and more extensive distribution of TR-Lip at the glioma foci, further confirming the targeting efficiency of TR-Lip (Figure 9B). The results could be explained as follows: (1) only a small amount of PEG-Lip and TH-Lip accumulated at the glioma foci, suggesting that they could not transport across the intact BBB; (2) as compared to RGD-Lip, TR-Lip could first faster transport across BBB by integrin $\alpha_v\beta_3$ on the surface of endothelial cells-mediated endocytosis and escaping from lysosomes, then more extensively distribute and deeper penetrate within glioma contributed by synergy effect of overexpressed integrin $\alpha_v\beta_3$ receptors on the surface of both glioma cells-mediated and electrostatic adsorption-mediated endocytosis; and (3) TR-Lip could escape from the reticuloendothelial system, especially liver, although it was rapidly internalized by liver in the early stage of blood circulation.

3.10. Anticancer Effect. Figure 10 showed anticancer efficacy in intracranial glioma-bearing mice. Kaplan−Meier survival curves (Figure 10A) indicated that the median survival time of mice treated with PTX-TR-Lip (45 days) was significantly longer than that of mice treated with PBS (20.5 days, $p < 0.001$), free PTX (25.5 days, $p < 0.001$), PTX-PEG-Lip

DOI: 10.1021/acsami.5b06429
ACS Appl. Mater. Interfaces 2015, 7, 21442−21454

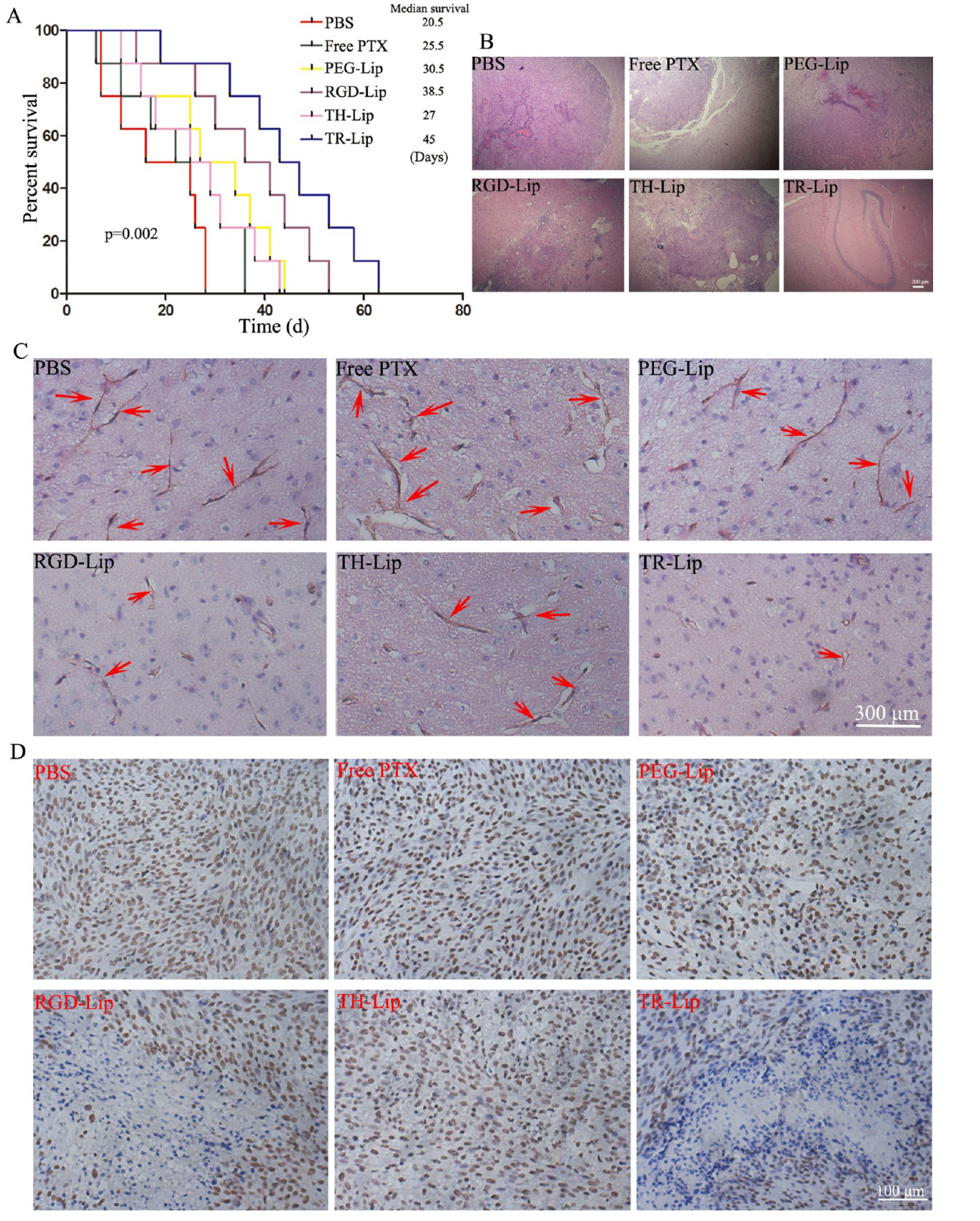

Figure 10. (A) Kaplan–Meier survival curves of C6 glioma-bearing mice treated with PTX-TR-Lip at day 6, 8, 10, 12, and 14 after inoculation (each dosing 3 mg/kg PTX). (B) H&E staining of brain glioma site. Scale bar, 200 μm. (C) CD34-PAS dual staining on the brain glioma site. Scale bar, 300 μm. (D) Immunohistochemical staining for CD133 on the brain glioma area. Scale bar, 100 μm.

(30.5 days, $p < 0.01$), PTX-RGD-Lip (38.5 days, $p < 0.05$), and PTX-TH-Lip (27 days, $p < 0.01$), respectively.

H&E staining (Figure 10B) demonstrated that PTX-TR-Lip after tail intravenous injection could prominently suppress the proliferation of C6 cells in vivo, although PTX-RGD-Lip also suppressed more cell proliferation as compared to other groups.

CD34-PAS dual staining (Figure 10C) depicted the destroying effect on the VM channels in slices of tumor masses after

DOI: 10.1021/acsami.5b06429
ACS Appl. Mater. Interfaces 2015, 7, 21442–21454

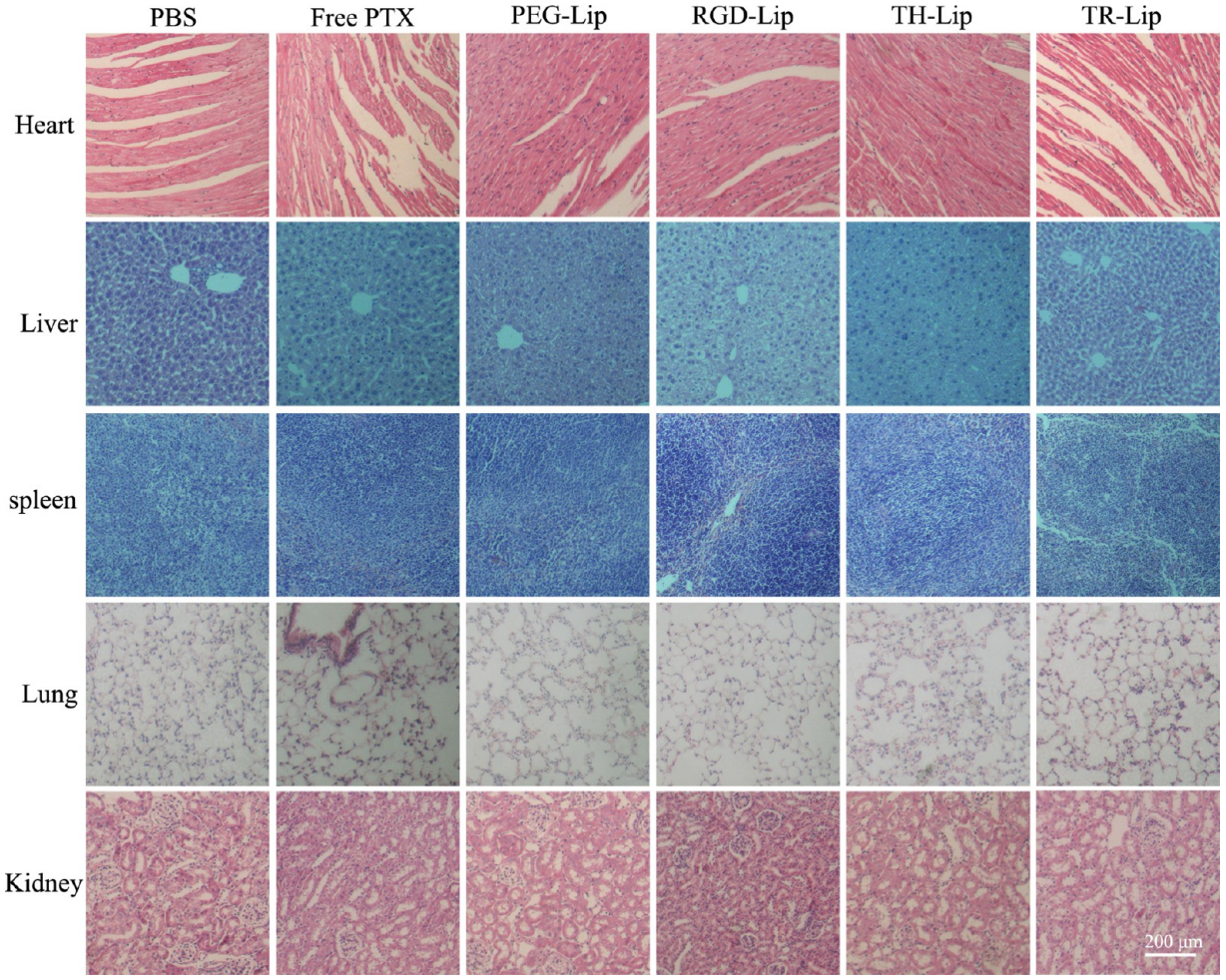

Figure 11. Histological evaluation of tissue from intracranial glioma-bearing mice after treatment with PBS, free PTX, PTX-PEG-Lip, PTX-RGD-Lip, PTX-TH-Lip, and PTX-TR-Lip (each dosing 3 mg/kg PTX). Tissues were stained with H&E. Scale bar, 200 μm.

treatment with PTX-loaded formulations. The rank of groups based on numbers of VM channels was PBS > free PTX > PTX−PEG-Lip ≈ PTX-TH-Lip > PTX-RGD-Lip > PTX-TR-Lip, suggesting that PTX-TR-Lip displayed the strongest destroying effect on the VM channels.

Figure 10D showed immunohistochemical staining for CD133 on the brain glioma area after treatment with PTX-loaded formulations. On the basis of the number of brain CSCs-expressed $CD133^+$, the rank of groups was PTX-TR-Lip < PTX-RGD-Lip < PTX-TH-Lip ≈ PTX−PEG-Lip ≈ free PTX ≈ PBS.

Histopathology observations were performed on the main organs from mice bearing brain glioma using H&E staining. There was no hyperemia, necrosis, or inflammation in heart, liver, spleen, lung, and kidney (Figure 11). In summary, no visible histopathological abnormalities or lesions were observed in any of the test groups, even free PTX group. All of these aspects above-mentioned contributed to the superior therapeutic efficacy of PTX-TR-Lip.

4. CONCLUSION

This study investigated several important aspects of TR-Lip during treating brain cancer with PTX: physical characteristics of liposomes, binding affinities to integrin $\alpha_v\beta_3$, transport across BBB, penetration in glioma spheroids, targeting efficacy in vivo, elimination of brain CSCs, and VM channels. The most significant anticancer efficacy in intracranial glioma-bearing mice was observed after the administration of PTX-TR-Lip. Enhanced therapeutic efficacy of PTX-TR-Lip in treating brain gliomas was related to the following reasons: (1) enhanced transport of TR-Lip across BBB indicated that more TR-Lip would be delivered to glioma; and (2) both excellent targeting efficiency and deep penetrating in glioma spheroids provided good opportunities for eliminating VM channels and brain CSCs. In multiple comparisons in vitro and in vivo by including free PTX, PTX-PEG-Lip, PTX-RGD-Lip, and PTX-TH-Lip as the controls, PTX-TR-Lip not only exhibited the strongest abilities for transferring liposomes across the BBB and for improving therapeutic efficacy in brain glioma-bearing animals, but also showed promise to reduce potential risks such as uncontrollable BBB leakage.

■ ASSOCIATED CONTENT

Supporting Information

The Supporting Information is available free of charge on the ACS Publications website at DOI: 10.1021/acsami.5b06429.

Figure S1: ^{1}H NMR spectrum of DSPE-PEG_{2000}-pepide in DMSO. Figure S2: Integrity of in vitro BBB model and the intracellular localization of liposomes across the in vitro BBB monolayer. Figure S3: Intracellular localization of CFPE-TR-Lip for C6 cells after treatment with different inhibitors at pH 6.5. Figure S4: Cellular uptake of CFPE-labeled liposomes in MCF-7 under different pH

DOI: 10.1021/acsami.5b06429
ACS Appl. Mater. Interfaces 2015, 7, 21442−21454

conditions. Figure S5: Cell viability (%) of C6 cells after treatment with four kinds of blank liposomes under different pH conditions (PDF)

AUTHOR INFORMATION

Corresponding Author

*Tel./fax: +86 28 85502532. E-mail: qinhe@scu.edu.cn.

Notes

The authors declare no competing financial interest.

ACKNOWLEDGMENTS

This work was funded by the National Basic Research Program of China (973 Program, 2013CB932504), the National Natural Science Foundation of China (81373337), and Sichuan Province Infrastructure Platform of Science and Technology (15010116).

REFERENCES

(1) Cohen, Z. R.; Ramishetti, S.; Peshes-Yaloz, N.; Goldsmith, M.; Wohl, A.; Zibly, Z.; Peer, D. Localized Rnai Therapeutics of Chemoresistant Grade Iv Glioma Using Hyaluronan-Grafted Lipid-Based Nanoparticles. *ACS Nano* **2015**, *9* (2), 1581−1591.

(2) Shao, K.; Ding, N.; Huang, S.; Ren, S.; Zhang, Y.; Kuang, Y.; Guo, Y.; Ma, H.; An, S.; Li, Y. Smart Nanodevice Combined Tumor-Specific Vector with Cellular Microenvironment-Triggered Property for Highly Effective Antiglioma Therapy. *ACS Nano* **2014**, *8* (2), 1191−1203.

(3) Ni, D.; Zhang, J.; Bu, W.; Xing, H.; Han, F.; Xiao, Q.; Yao, Z.; Chen, F.; He, Q.; Liu, J. Dual-Targeting Upconversion Nanoprobes across the Blood−Brain Barrier for Magnetic Resonance/Fluorescence Imaging of Intracranial Glioblastoma. *ACS Nano* **2014**, *8* (2), 1231−1242.

(4) Ting, C.-Y.; Fan, C.-H.; Liu, H.-L.; Huang, C.-Y.; Hsieh, H.-Y.; Yen, T.-C.; Wei, K.-C.; Yeh, C.-K. Concurrent Blood−Brain Barrier Opening and Local Drug Delivery Using Drug-Carrying Microbubbles and Focused Ultrasound for Brain Glioma Treatment. *Biomaterials* **2012**, *33* (2), 704−712.

(5) Shi, K.; Zhou, J.; Zhang, Q.; Gao, H.; Liu, Y.; Zong, T.; He, Q. Arginine-Glycine-Aspartic Acid-Modified Lipid-Polymer Hybrid Nanoparticles for Docetaxel Delivery in Glioblastoma Multiforme. *J. Biomed. Nanotechnol.* **2015**, *11* (3), 382−391.

(6) Miura, Y.; Takenaka, T.; Toh, K.; Wu, S.; Nishihara, H.; Kano, M. R.; Ino, Y.; Nomoto, T.; Matsumoto, Y.; Koyama, H. Cyclic Rgd-Linked Polymeric Micelles for Targeted Delivery of Platinum Anticancer Drugs to Glioblastoma through the Blood−Brain Tumor Barrier. *ACS Nano* **2013**, *7* (10), 8583−8592.

(7) Li, X.-Y.; Zhao, Y.; Sun, M.-G.; Shi, J.-F.; Ju, R.-J.; Zhang, C.-X.; Li, X.-T.; Zhao, W.-Y.; Mu, L.-M.; Zeng, F. Multifunctional Liposomes Loaded with Paclitaxel and Artemether for Treatment of Invasive Brain Glioma. *Biomaterials* **2014**, *35* (21), 5591−5604.

(8) Vescovi, A. L.; Galli, R.; Reynolds, B. A. Brain Tumour Stem Cells. *Nat. Rev. Cancer* **2006**, *6* (6), 425−436.

(9) Garofalo, M.; Croce, C. M. Role of Micrornas in Maintaining Cancer Stem Cells. *Adv. Drug Delivery Rev.* **2015**, *81*, 53−61.

(10) Zhang, S.; Zhang, D.; Sun, B. Vasculogenic Mimicry: Current Status and Future Prospects. *Cancer Lett.* **2007**, *254* (2), 157−164.

(11) Hendrix, M. J.; Seftor, E. A.; Hess, A. R.; Seftor, R. E. Vasculogenic Mimicry and Tumour-Cell Plasticity: Lessons from Melanoma. *Nat. Rev. Cancer* **2003**, *3* (6), 411−421.

(12) Francescone, R.; Scully, S.; Bentley, B.; Yan, W.; Taylor, S. L.; Oh, D.; Moral, L.; Shao, R. Glioblastoma-Derived Tumor Cells Induce Vasculogenic Mimicry through Flk-1 Protein Activation. *J. Biol. Chem.* **2012**, *287* (29), 24821−24831.

(13) Liu, Y.; Ran, R.; Chen, J.; Kuang, Q.; Tang, J.; Mei, L.; Zhang, Q.; Gao, H.; Zhang, Z.; He, Q. Paclitaxel Loaded Liposomes Decorated with a Multifunctional Tandem Peptide for Glioma Targeting. *Biomaterials* **2014**, *35* (17), 4835−4847.

(14) Liu, Y.; Ji, M.; Wong, M. K.; Joo, K.-I.; Wang, P. Enhanced Therapeutic Efficacy of Irgd-Conjugated Crosslinked Multilayer Liposomes for Drug Delivery. *BioMed Res. Int.* **2013**, *2013*, 1.

(15) Zhan, C.; Gu, B.; Xie, C.; Li, J.; Liu, Y.; Lu, W. Cyclic Rgd Conjugated Poly (Ethylene Glycol)-Co-Poly (Lactic Acid) Micelle Enhances Paclitaxel Anti-Glioblastoma Effect. *J. Controlled Release* **2010**, *143* (1), 136−142.

(16) Choi, N.; Kim, S.-M.; Hong, K. S.; Cho, G.; Cho, J.-H.; Lee, C.; Ryu, E. K. The Use of the Fusion Protein Rgd-Hsa-Timp2 as a Tumor Targeting Imaging Probe for Spect and Pet. *Biomaterials* **2011**, *32* (29), 7151−7158.

(17) Zhang, F.; Huang, X.; Zhu, L.; Guo, N.; Niu, G.; Swierczewska, M.; Lee, S.; Xu, H.; Wang, A. Y.; Mohamedali, K. A. Noninvasive Monitoring of Orthotopic Glioblastoma Therapy Response Using Rgd-Conjugated Iron Oxide Nanoparticles. *Biomaterials* **2012**, *33* (21), 5414−5422.

(18) Burgett, M. E.; Huang, P.; Tipps, R. S.; Vasanji, A.; Lathia, J. D.; Li, M.; Bao, S.; Rich, J. N.; Gladson, C. L. Glioma Stem Cells Promote Brain Endothelial Cell Motility: A New Mechanism for the Direct Interaction of Glioma Stem Cells with Endothelial Cells. *Cancer Res.* **2013**, *73*, 3898−3898.

(19) Wang, K.; Zhang, X.; Liu, Y.; Liu, C.; Jiang, B.; Jiang, Y. Tumor Penetrability and Anti-Angiogenesis Using Irgd-Mediated Delivery of Doxorubicin-Polymer Conjugates. *Biomaterials* **2014**, *35* (30), 8735−8747.

(20) Zhang, Q.; Tang, J.; Fu, L.; Ran, R.; Liu, Y.; Yuan, M.; He, Q. A Ph-Responsive A-Helical Cell Penetrating Peptide-Mediated Liposomal Delivery System. *Biomaterials* **2013**, *34* (32), 7980−7993.

(21) Yu, X.; Yang, X.; Horte, S.; Kizhakkedathu, J. N.; Brooks, D. E. A Ph and Thermosensitive Choline Phosphate-Based Delivery Platform Targeted to the Acidic Tumor Microenvironment. *Biomaterials* **2014**, *35* (1), 278−286.

(22) Zhang, W.; Song, J.; Zhang, B.; Liu, L.; Wang, K.; Wang, R. Design of Acid-Activated Cell Penetrating Peptide for Delivery of Active Molecules into Cancer Cells. *Bioconjugate Chem.* **2011**, *22* (7), 1410−1415.

(23) Yuba, E.; Tajima, N.; Yoshizaki, Y.; Harada, A.; Hayashi, H.; Kono, K. Dextran Derivative-Based Ph-Sensitive Liposomes for Cancer Immunotherapy. *Biomaterials* **2014**, *35* (9), 3091−3101.

(24) Liu, Y.; Kim, Y. J.; Ji, M.; Fang, J.; Siriwon, N.; Zhang, L. I.; Wang, P. Enhancing Gene Delivery of Adeno-Associated Viruses by Cell-Permeable Peptides. *Mol. Ther.–Methods Clin. Dev.* **2014**, *1*, 12.

(25) Canovi, M.; Markoutsa, E.; Lazar, A. N.; Pampalakis, G.; Clemente, C.; Re, F.; Sesana, S.; Masserini, M.; Salmona, M.; Duyckaerts, C. The Binding Affinity of Anti-Aβ1−42 Mab-Decorated Nanoliposomes to Aβ1−42 Peptides in Vitro and to Amyloid Deposits in Post-Mortem Tissue. *Biomaterials* **2011**, *32* (23), 5489−5497.

(26) Schneider, C. S.; Perez, J. G.; Cheng, E.; Zhang, C.; Mastorakos, P.; Hanes, J.; Winkles, J. A.; Woodworth, G. F.; Kim, A. J. Minimizing the Non-Specific Binding of Nanoparticles to the Brain Enables Active Targeting of Fn14-Positive Glioblastoma Cells. *Biomaterials* **2015**, *42*, 42−51.

(27) Ying, X.; Wen, H.; Lu, W.-L.; Du, J.; Guo, J.; Tian, W.; Men, Y.; Zhang, Y.; Li, R.-J.; Yang, T.-Y. Dual-Targeting Daunorubicin Liposomes Improve the Therapeutic Efficacy of Brain Glioma in Animals. *J. Controlled Release* **2010**, *141* (2), 183−192.

(28) Xie, Y.; Ye, L.; Zhang, X.; Cui, W.; Lou, J.; Nagai, T.; Hou, X. Transport of Nerve Growth Factor Encapsulated into Liposomes across the Blood−Brain Barrier: In Vitro and in Vivo Studies. *J. Controlled Release* **2005**, *105* (1), 106−119.

(29) Booth, R.; Kim, H. Permeability Analysis of Neuroactive Drugs through a Dynamic Microfluidic in Vitro Blood−Brain Barrier Model. *Ann. Biomed. Eng.* **2014**, *42* (12), 2379−2391.

(30) Gao, X.; Qian, J.; Zheng, S.; Changyi, Y.; Zhang, J.; Ju, S.; Zhu, J.; Li, C. Overcoming the Blood−Brain Barrier for Delivering Drugs into the Brain by Using Adenosine Receptor Nanoagonist. *ACS Nano* **2014**, *8* (4), 3678−3689.

(31) Wang, K.; Zhang, X.; Liu, Y.; Liu, C.; Jiang, B.; Jiang, Y. Tumor Penetrability and Anti-Angiogenesis Using Irgd-Mediated Delivery of Doxorubicin-Polymer Conjugates. *Biomaterials* **2014**, *35* (30), 8735−8747.

DOI: 10.1021/acsami.5b06429
ACS Appl. Mater. Interfaces 2015, 7, 21442−21454

(32) Hu, Q.; Gao, X.; Gu, G.; Kang, T.; Tu, Y.; Liu, Z.; Song, Q.; Yao, L.; Pang, Z.; Jiang, X. Glioma Therapy Using Tumor Homing and Penetrating Peptide-Functionalized Peg−Pla Nanoparticles Loaded with Paclitaxel. *Biomaterials* **2013**, *34* (22), 5640−5650.
(33) Liu, Y.; Ran, R.; Chen, J.; Kuang, Q.; Tang, J.; Mei, L.; Zhang, Q.; Gao, H.; Zhang, Z.; He, Q. Paclitaxel Loaded Liposomes Decorated with a Multifunctional Tandem Peptide for Glioma Targeting. *Biomaterials* **2014**, *35* (17), 4835−4847.
(34) Wang, D.; Guo, Y.; Li, Y.; Li, W.; Zheng, X.; Xia, H.; Mao, Q. Detection of CD133 Expression in U87 Glioblastoma Cells Using a Novel Anti-Cd133 Monoclonal Antibody. *Oncol. Lett.* **2015**, *3079*, 2603−2608.
(35) Zhang, Q.; Tang, J.; Fu, L.; Ran, R.; Liu, Y.; Yuan, M.; He, Q. A pH-Responsive α-Helical Cell Penetrating Peptide-Mediated Liposomal Delivery System. *Biomaterials* **2013**, *34* (32), 7980−7993.
(36) Park, T.-E.; Singh, B.; Li, H.; Lee, J.-Y.; Kang, S.-K.; Choi, Y.-J.; Cho, C.-S. Enhanced Bbb Permeability of Osmotically Active Poly (Mannitol-Co-Pei) Modified with Rabies Virus Glycoprotein Via Selective Stimulation of Caveolar Endocytosis for Rnai Therapeutics in Alzheimer's Disease. *Biomaterials* **2015**, *38*, 61−71.
(37) Chen, Y.; Liu, L. Modern Methods for Delivery of Drugs across the Blood−Brain Barrier. *Adv. Drug Delivery Rev.* **2012**, *64* (7), 640−665.
(38) Tabatabaei, S. N.; Girouard, H.; Carret, A.-S.; Martel, S. Remote Control of the Permeability of the Blood−Brain Barrier by Magnetic Heating of Nanoparticles: A Proof of Concept for Brain Drug Delivery. *J. Controlled Release* **2015**, *206*, 49−57.
(39) Cheng, S.-H.; Lee, C.-H.; Chen, M.-C.; Souris, J. S.; Tseng, F.-G.; Yang, C.-S.; Mou, C.-Y.; Chen, C.-T.; Lo, L.-W. Tri-Functionalization of Mesoporous Silica Nanoparticles for Comprehensive Cancer Theranostics—the Trio of Imaging, Targeting and Therapy. *J. Mater. Chem.* **2010**, *20* (29), 6149−6157.
(40) Ko, H. Y.; Choi, K.-J.; Lee, C. H.; Kim, S. A Multimodal Nanoparticle-Based Cancer Imaging Probe Simultaneously Targeting Nucleolin, Integrin A V B 3 and Tenascin-C Proteins. *Biomaterials* **2011**, *32* (4), 1130−1138.
(41) Yamano, S.; Dai, J.; Hanatani, S.; Haku, K.; Yamanaka, T.; Ishioka, M.; Takayama, T.; Yuvienco, C.; Khapli, S.; Moursi, A. M. Long-Term Efficient Gene Delivery Using Polyethylenimine with Modified Tat Peptide. *Biomaterials* **2014**, *35* (5), 1705−1715.
(42) Lim, J. P.; Gleeson, P. A. Macropinocytosis: An Endocytic Pathway for Internalising Large Gulps. *Immunol. Cell Biol.* **2011**, *89* (8), 836−843.
(43) Gu, G.; Hu, Q.; Feng, X.; Gao, X.; Menglin, J.; Kang, T.; Jiang, D.; Song, Q.; Chen, H.; Chen, J. Peg-Pla Nanoparticles Modified with Aptedb Peptide for Enhanced Anti-Angiogenic and Anti-Glioma Therapy. *Biomaterials* **2014**, *35* (28), 8215−8226.
(44) Jiang, X.; Sha, X.; Xin, H.; Chen, L.; Gao, X.; Wang, X.; Law, K.; Gu, J.; Chen, Y.; Jiang, Y.; Ren, X.; Ren, Q.; Fang, X. Self-Aggregated Pegylated Poly (Trimethylene Carbonate) Nanoparticles Decorated with C(Rgdyk) Peptide for Targeted Paclitaxel Delivery to Integrin-Rich Tumors. *Biomaterials* **2011**, *32* (35), 9457−9469.
(45) Markman, J. L.; Rekechenetskiy, A.; Holler, E.; Ljubimova, J. Y. Nanomedicine Therapeutic Approaches to Overcome Cancer Drug Resistance. *Adv. Drug Delivery Rev.* **2013**, *65* (13), 1866−1879.
(46) Ju, R.-J.; Li, X.-T.; Shi, J.-F.; Li, X.-Y.; Sun, M.-G.; Zeng, F.; Zhou, J.; Liu, L.; Zhang, C.-X.; Zhao, W.-Y. Liposomes, Modified with Ptd Hiv-1 Peptide, Containing Epirubicin and Celecoxib, to Target Vasculogenic Mimicry Channels in Invasive Breast Cancer. *Biomaterials* **2014**, *35* (26), 7610−7621.
(47) Mehta, G.; Hsiao, A. Y.; Ingram, M.; Luker, G. D.; Takayama, S. Opportunities and Challenges for Use of Tumor Spheroids as Models to Test Drug Delivery and Efficacy. *J. Controlled Release* **2012**, *164* (2), 192−204.

DOI: 10.1021/acsami.5b06429
ACS Appl. Mater. Interfaces 2015, 7, 21442−21454